Asymptotic analysis of combined breather-kink modes in a Fermi-Pasta-Ulam chain

Imran A Butt Jonathan A D Wattis

Theoretical Mechanics, School of Mathematical Sciences, University of Nottingham, University Park, Nottingham, NG7 2RD, UK.

15 July 2008

Abstract

We find approximations to travelling breather solutions of the one-dimensional Fermi-Pasta-Ulam (FPU) lattice. Both bright breather and dark breather solutions are found. We find that the existence of localised (bright) solutions depends upon the coefficients of cubic and quartic terms of the potential energy, generalising an earlier inequality derived by James [CR Acad Sci Paris 332, 581, (2001)]. We use the method of multiple scales to reduce the equations of motion for the lattice to a nonlinear Schrödinger equation at leading order and hence construct an asymptotic form for the breather. We show that in the absence of a cubic potential energy term, the lattice supports combined breathing-kink waveforms. The amplitude of breathing-kinks can be arbitrarily small, as opposed to traditional monotone kinks, which have a nonzero minimum amplitude in such systems. We also present numerical simulations of the lattice, verifying the shape and velocity of the travelling waveforms, and confirming the long-lived nature of all such modes.

Key words: breathers, nonlinear waves, discrete systems,
PACS: 05.45.-a, 05.45.Yv

1 Introduction

Discrete breathers are time-periodic and spatially localised solutions of coupled chains of nonlinear oscillators. In 1994, Mackay and Aubry [18] established the existence of stationary breathers in a broad range of lattice models. In their method, breathers are obtained by continuation from the anti-continuum limit

Email addresses: imran.butt@maths.nottingham.ac.uk, Jonathan.Wattis@nottingham.ac.uk (Jonathan A D Wattis).

at which the network is reduced to an array of uncoupled oscillators. In this limit, breathers are found trivially, since one may take breathers for which only one oscillator is excited, and the others remain at rest.

This method is not applicable to Fermi-Pasta-Ulam (FPU) lattices of the type first investigated by Fermi *et al.* [8], since these do not possess an uncoupled limit in which trivial breathers exist. Nevertheless, early analytical and numerical work indicated that FPU lattices could indeed support breathers, see for instance, Takeno [28] and Bickham *et al.* [3]. Later, rigorous proofs for existence in particular FPU models were provided by Flach [9] and Aubry *et al.* [1].

James [17] presents a proof of the existence (nonexistence) of breathers in general FPU lattices provided that the interaction potential satisfies (violates) a local hardening condition. Small amplitude breathers with frequencies slightly above the phonon band are found when $B > 0$, where $B = V^{(4)}(0)/2 - (V^{(3)}(0))^2$, and their nonexistence is proved for $B < 0$ (V is the interaction potential, and is chosen to satisfy $V'(0) = 0$ and $V''(0) = 1$). Accompanying numerical work by Sanchez-Ray *et al.* [23] illustrates the range of validity of James' centre manifold technique since small amplitude breathers are computed and found to be in good agreement with leading-order analytical expressions deduced by James.

Whilst we know of no proofs for the existence of moving breathers in lattices, their long-lived nature has been noted, and has inspired more detailed study of their stability and mobility. Sandusky *et al.* [24] use a combination of the rotating-wave approximation (RWA) to describe the temporal evolution of a breather, together with a numerical solution of its shape. Two types of stationary breather are found; one centred on a lattice site and one centred between lattice sites. Numerical simulations and heuristic arguments show that the former is unstable to perturbations which caused motion of the breather. The latter type is found to be stable. These results thus show that breathers (as well as kinks) experience a type of Peierls-Nabarro potential barrier; however, the concept of an energy barrier is not as useful for breathers as kinks, since its amplitude depends on the internal phase of the breather (as shown in [32]).

In this paper, we use asymptotic methods to find leading-order expressions for the form of breathers in a one-dimensional Fermi-Pasta-Ulam chain with anharmonic potential. In Section 2 we apply the semi-discrete multiple-scale method of Remoissenet [19] to reduce the governing equations to a nonlinear Schrödinger (NLS) at leading order. The validity of this method has since been established by Schneider & Wayne [25], and by Giannoulis and Mielke [12, 13] for a more general form of equation in which there is an on-site potential as well as the nearest-neighbour interactions. The NLS equation admits two different types of soliton solution (bright or dark) for the breather envelope,

depending upon the coefficients of the cubic and quartic terms in the potential energy function. Our asymptotic analysis yields inequalities which illustrate how the size of these coefficients determine the type of solution. This leads to conditions for which the FPU lattice supports bright or dark breathers in the lattice. We find that stationary breathers satisfy James' inequality $B > 0$, while for moving breathers, we find a generalised version of James' inequality. Soliton solutions of the NLS equation are used to construct leading-order analytic forms for bright and dark breathers in the FPU chain. We present results of numerical simulations of the FPU lattice in Section 3 we find good agreement with the results predicted by the asymptotic analysis.

In Section 4, we show, by considering small wavenumbers, that there also exist waveforms which are combinations of a breather and a kink. The order of magnitude of the wavenumber determines which of the two components dominates in such a waveform, and hence whether a breather or a kink or a combined breathing-kink is exhibited ultimately. We present numerical simulations which show that these combined modes move as travelling waves over intermediate timescales. We show that traditional, monotone, kinks in the quartic FPU lattice have a non-zero minimum amplitude, and that the combined modes allow travelling waves with a kink amplitude below this minimum. Whilst Flytzanis *et al.* [10] found approximations to combined travelling breather-kinks in this system, their solution ansatz explicitly assumes the existence of both an oscillatory (breather) and a slowly varying (kink) components with similar amplitudes. Our approach is to work with a different formulation of the problem, and use a solution ansatz which has only an oscillatory component. The existence of a slowly varying component (which has the form of a kink) then arises naturally and the amplitude of this resultant mode is determined as part of the problem. A brief summary and some closing comments are given in Section 5. In particular, we discuss several merits of the methodology used in this paper over other early analytic methods applied to similar lattice models, such as the rotating-wave approximation.

2 The Fermi-Pasta-Ulam lattice

2.1 Preliminaries

We restrict our attention to the one-dimensional FPU lattice. In such a lattice, particles interact with their nearest neighbours. The variable q_n denotes the displacement of the nth particle from its equilibrium position. The Hamil-

tonian of this system is given by

$$H = \sum_{n=-\infty}^{\infty} \left(\tfrac{1}{2}\dot{q}_n^2 + V(q_{n+1} - q_n) \right), \tag{1}$$

where V is the potential due to nearest neighbour interactions, and the index n runs over the entire one-dimensional lattice. The Hamiltonian (1) yields the equations of motion

$$\ddot{q}_n(t) = V'(q_{n+1} - q_n) - V'(q_n - q_{n-1}). \tag{2}$$

At this point, we introduce the variable ϕ_n, defined as the difference between the displacements of the $(n+1)$th and nth particles, namely

$$\phi_n = q_{n+1} - q_n. \tag{3}$$

In terms of the new variable ϕ_n, (2) becomes

$$\ddot{\phi}_n = V'(\phi_{n+1}) - 2V'(\phi_n) + V'(\phi_{n-1}). \tag{4}$$

Since we shall be using asymptotic methods to determine the form of small amplitude solutions, we are only be concerned with the first few terms in the expansion of $V(\phi)$. Thus we define the potential function $V(\phi)$ by

$$V'(\phi) = \tfrac{1}{2}\phi^2 + \tfrac{1}{3}a\phi^3 + \tfrac{1}{4}b\phi^4, \tag{5}$$

where a and b are real constants. The equations of motion (4) therefore become

$$\ddot{\phi}_n = (\phi_{n+1} - 2\phi_n + \phi_{n-1}) + a(\phi_{n+1}^2 - 2\phi_n^2 + \phi_{n-1}^2) + b(\phi_{n+1}^3 - 2\phi_n^3 + \phi_{n-1}^3). \tag{6}$$

Since we seek localised solutions, we expect the energy to vanish as $n \to \pm\infty$, hence we impose the boundary conditions $q_n \to 0$ as $n \to -\infty$ and $q_n \to q_\infty$ as $n \to +\infty$ for some constant $q_\infty \in \mathbb{R}$. Recalling the definition of ϕ_n in terms of q_n in (3), we find

$$q_n = \sum_{k=-\infty}^{n-1} \phi_k, \tag{7}$$

hence we express the latter boundary condition as

$$q_n \to q_\infty = \sum_{n=-\infty}^{\infty} \phi_n \quad \text{as} \quad n \to \infty. \tag{8}$$

We shall, in general, consider both $q_\infty = 0$ and $q_\infty \neq 0$ so that the variable q_n describes a modulated pulse ($q_\infty = 0$) or a modulated kink ($q_\infty \neq 0$) of some form.

We restrict our attention to a specific class of breather solutions, namely those of small amplitude (in ϕ), and whose envelope varies slowly compared to that of the carrier oscillations. For such solutions, we apply the method of asymptotic expansions with multiple space and time scales (see Remoissenet [19, 20]) to determine approximations to breather solutions. Hence, in addition to the variables n and t, we introduce new slow variables X, τ and T defined by

$$X = \varepsilon n, \quad \tau = \varepsilon t \quad \text{and} \quad T = \varepsilon^2 t. \tag{9}$$

We consider the displacement $\phi_n(t)$ to be a function of the independent variables n, t, X, τ and T so that $\phi_n(t) = \phi(n, t, X, \tau, T)$. Applying the chain rule for partial differentiation, the derivative operator $\mathrm{d}/\mathrm{d}t$ is replaced by

$$\frac{\mathrm{d}}{\mathrm{d}t} \equiv \frac{\partial}{\partial t} + \varepsilon\frac{\partial}{\partial \tau} + \varepsilon^2\frac{\partial}{\partial T}. \tag{10}$$

We assume a small-amplitude asymptotic expansion for modulated solutions of (6) of the form

$$\begin{aligned}\phi_n(t) = {} & \varepsilon \mathrm{e}^{\mathrm{i}\omega t + \mathrm{i}pn} F(X,\tau,T) + \varepsilon^2 G_0(X,\tau,T) \\ & + \varepsilon^2 \mathrm{e}^{\mathrm{i}\omega t + \mathrm{i}pn} G_1(X,\tau,T) + \varepsilon^2 \mathrm{e}^{2\mathrm{i}\omega t + 2\mathrm{i}pn} G_2(X,\tau,T) \\ & + \varepsilon^3 H_0(X,\tau,T) + \varepsilon^3 \mathrm{e}^{\mathrm{i}\omega t + \mathrm{i}pn} H_1(X,\tau,T) \\ & + \varepsilon^3 \mathrm{e}^{2\mathrm{i}\omega t + 2\mathrm{i}pn} H_2(X,\tau,T) + \varepsilon^3 \mathrm{e}^{3\mathrm{i}\omega t + 3\mathrm{i}pn} H_3(X,\tau,T) + \cdots + \text{c.c.},\end{aligned} \tag{11}$$

where c.c. denotes the complex conjugate, and ω and p are the frequency and wavenumber of the linear carrier wave respectively. We substitute the ansatz (11) into the equations of motion (6) and equate coefficients of each harmonic in t at each order of ε. This yields the following equations:

$\mathcal{O}(\varepsilon \mathrm{e}^{\mathrm{i}\omega t + \mathrm{i}pn})$:

$$-\omega^2 F = \mathrm{e}^{\mathrm{i}p} F + \mathrm{e}^{-\mathrm{i}p} F - 2F, \tag{12}$$

$\mathcal{O}(\varepsilon^2 \mathrm{e}^{\mathrm{i}\omega t + \mathrm{i}pn})$:

$$\omega F_\tau = \sin(p) F_X, \tag{13}$$

$\mathcal{O}(\varepsilon^2 \mathrm{e}^{2\mathrm{i}\omega t + 2\mathrm{i}pn})$:

$$\omega^2 G_2 = \sin^2(p)(G_2 + aF^2), \tag{14}$$

$\mathcal{O}(\varepsilon^3 \mathrm{e}^{\mathrm{i}\omega t + \mathrm{i}pn})$:

$$\begin{aligned}2\mathrm{i}\omega F_T + F_{\tau\tau} + 2\mathrm{i}\omega G_{1\tau} = {} & \cos(p) F_{XX} + 2\mathrm{i}\sin(p) G_{1X} \\ & - 8a \sin^2\left(\frac{p}{2}\right)\left[F G_0 + F\overline{G}_0 + \overline{F} G_2\right] \\ & - 12b \sin^2\left(\frac{p}{2}\right)|F|^2 F,\end{aligned} \tag{15}$$

$\mathcal{O}(\varepsilon^4 \mathrm{e}^0)$:

$$G_{0\tau\tau} = G_{0XX} + a\left(|F|^2\right)_{XX}. \tag{16}$$

The equation from $\mathcal{O}(\varepsilon^2 \mathrm{e}^0)$ is trivial so is discarded. We proceed to solve the above set of equations. Equation (12) yields the dispersion relation $\omega^2 = 4\sin^2(p/2)$, from which we conclude that

$$\omega = 2\sin\left(\frac{p}{2}\right). \tag{17}$$

Considering (13), after substituting for ω from (17), this becomes

$$F_\tau = \cos\left(\frac{p}{2}\right) F_X, \tag{18}$$

from which we infer that F is a travelling wave of the form

$$F(X, \tau, T) \equiv F(Z, T), \tag{19}$$

where $Z = X - v\tau$ and the velocity $v = -\cos(p/2)$. Thus, for $p = \pi$ we have a stationary wave, and for other values of p a wave which moves with speed below unity.

Equation (14) is an algebraic equation, which is solved easily to give G_2 in terms of F

$$G_2 = a\cot^2\left(\frac{p}{2}\right) F^2. \tag{20}$$

Note that for stationary waves (which occur when $p = \pi$), there is no generation of a second harmonic. Note also that when $a \neq 0$ the expression for G_2 becomes singular as $p \to 0$. In particular, from (20), we see that if $p = \mathcal{O}(\varepsilon^{1/2})$ or smaller, then the F term in (11) is not dominant, but of similar size to the G_2 term.

Turning our attention to (15), we anticipate that this should reduce to a nonlinear Schrödinger (NLS) equation in the variable F, as is the case for other lattice models (see for example, Remoissenet [19], Bang & Peyrard [2], and Wattis [33]). However, at present, it is clear that (15) also includes terms involving G_1 and G_0. These must be found in terms of F before reduction to the NLS equation can occur.

The quantities G_1 and G_0 are higher-order correction terms to the leading order quantity F. If we assume that G_1 and G_0 represent perturbations travelling at the same velocity as F, we have that

$$G_1(X, \tau, T) = G_1(Z, T) \quad \text{and} \quad G_0(X, \tau, T) = G_0(Z, T), \tag{21}$$

where as before, $Z = X - v\tau$ and $v = -\cos(p/2)$. It follows from the left-hand equality in (21) that the terms involving G_1 on either side of (15) disappear.

Also, using the right-hand equality in (21), we find that $G_{0\tau\tau} = v^2 G_{0ZZ}$, and so equation (16) becomes

$$(v^2 - 1)G_{0ZZ} = a(|F|^2)_{ZZ}. \tag{22}$$

Integrating this equation twice with respect to Z gives

$$G_0 = \frac{a}{v^2 - 1}|F|^2 = -a \operatorname{cosec}^2\left(\frac{p}{2}\right)|F|^2. \tag{23}$$

Note that in (23), we have taken the constants of integration to be zero. This follows from the comments regarding boundary conditions made immediately after (6). Also, again, we see that the expression for G_0 (23) becomes singular as $p \to 0$.

We now return to (15). Substituting for G_2 and G_0 using (20) and (23) respectively, we arrive the NLS equation for F as anticipated

$$\mathrm{i}F_T + PF_{ZZ} + Q|F|^2F = 0. \tag{24}$$

In (24), the coefficients P and Q of F_{ZZ} and $|F|^2F$ respectively are given by

$$P = \tfrac{1}{4}\sin\left(\frac{p}{2}\right) \quad \text{and} \quad Q = \frac{2a^2\cos^2\left(\frac{p}{2}\right) - 4a^2 + 3b\sin^2\left(\frac{p}{2}\right)}{\sin\left(\frac{p}{2}\right)}. \tag{25}$$

In other words, the multiple-scale ansatz (11) reduces the FPU equations (6) defined upon a discrete chain to a continuum partial differential equation (the NLS equation, (24)) for the breather envelope F. The next task is to determine soliton solutions of (24) which give an analytic formula for the envelope F.

2.3 Bright soliton solutions

It is known that the nonlinear Schrödinger equation (24) admits bright soliton solutions (also known as envelope solitons) if the coefficients P and Q are of the same sign, and dark solitons (also known as hole solitons) if P and Q are of opposite sign (see Remoissenet [20] and Scott [26], for example). Clearly P is positive for all p in the interval $[0, 2\pi]$ (except at $p = 0$ and $p = 2\pi$). Hence for bright soliton solutions, the above condition reduces to $Q > 0$, which upon rearranging becomes

$$\left(\frac{3b}{2a^2} - 1\right)\sin^2\left(\frac{p}{2}\right) > 1. \tag{26}$$

Inequality (26) is critical for determining the existence and nonexistence of stationary discrete breathers and long-lived moving breather modes in the one-dimensional FPU chain. In analysing this inequality, it is instructive to

consider the (a, b)-parameter-space. For a fixed wavenumber p, we see that in order for the inequality to be satisfied, b must be greater than some simple quadratic function of a, namely

$$b > \frac{2}{3}\left[\mathrm{cosec}^2\left(\frac{p}{2}\right) + 1\right] a^2. \tag{27}$$

This inequality is illustrated in Figure 1, which shows the inequality (27) for four distinct wavenumbers $p = j\pi/4$ with $j = 1, 2, 3, 4$. For any given value of a, the lowest possible value of b satisfying (27) occurs when $p = \pi$ (that is, when $\mathrm{cosec}^2(p/2)$ takes its minimum value of 1). For this wavenumber, for which breathers are stationary, we have $b > \frac{4}{3}a^2$. This is exactly the inequality proven by James [17] for the existence of stationary breathers that we discussed in Section 1. From (5), we find that $V^{(3)}(0) = 2a$ and $V^{(4)}(0) = 6b$. Hence James' condition for breather existence in the FPU chain gives $B = 3b - 4a^2 > 0$, which is the same inequality that we arrive at above.

This inequality tells us that no bright breathers exist below the curve which corresponds to $p = \pi$ (see Figure 1), and so this is effectively a necessary condition for breather existence in the 1D FPU chain.

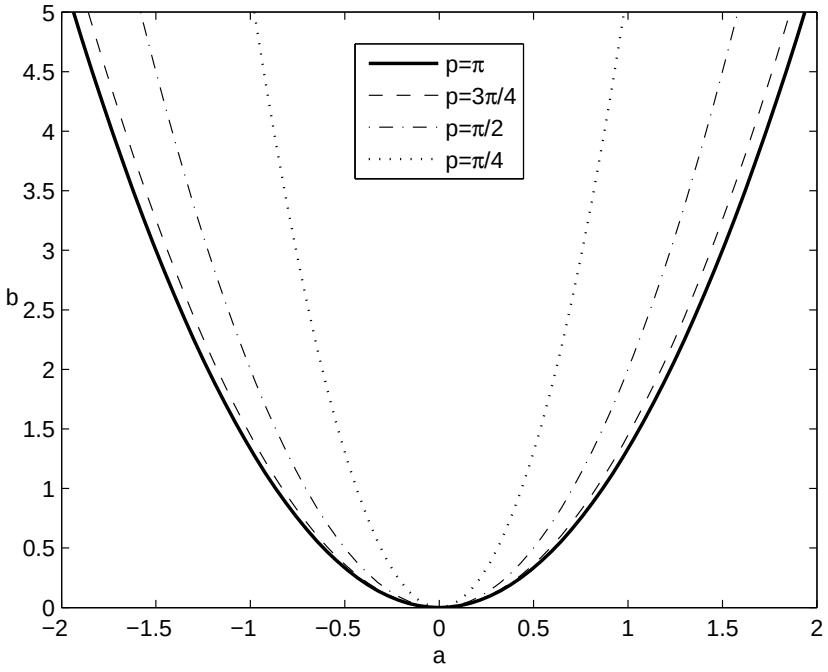

Fig. 1. Illustration of the inequality (27) (see text for explanation).

Returning to the remaining curves in Figure 1 for a moment, we comment that above the solid curve, stationary breathers with $p = \pi$ exist. Similarly, above the dashed curve $(--)$, we expect to find bright breathers with $p \geq 3\pi/4$.

These are slowly moving modes, since $|v| < \cos(3\pi/8) \approx 0.38$ units per second. Above the dash-dotted curve $(-\cdot)$, breathers with $p \geq \pi/2$ exist; these move with speed $|v| < 1/\sqrt{2} \approx 0.707$ units per second. Above the dotted curve $(\cdots)$, breathers with $p \geq \pi/4$ exist. These travel with speed $|v| < \cos(\pi/8) \approx 0.92$ units per second. For each wavenumber p a similar parabola is generated. If we choose to consider arbitrarily small wavenumbers, then it is clear from (27) that small amplitude breathers exist only in a neighbourhood of the b-axis, that is, when $b \gg a$.

Given (a, b) satisfying the condition for a *moving* breather with wavenumber p, namely (27), then we also expect to find breathers with larger p-values, and in particular $p = \pi$ and hence a *stationary* breather mode to exist. A rearrangement of (26) shows there is a threshold wavenumber, $p_{\min}$, above which the inequality (26) is satisfied. Explicitly, for bright soliton solutions, the wavenumber p must satisfy $p_{\min} < p \leq \pi$ where

$$p_{\min} = 2\sin^{-1}\sqrt{\frac{2a^2}{3b - 2a^2}}. \tag{28}$$

In Section 3, we investigate the properties of breathers which correspond to wavenumber p, where $p \to p_{\min}^{+}$. For now, we note that if we consider the special case of a lattice with symmetric quartic potential ($a = 0$), then from (25), we see that the condition $Q > 0$ reduces to $b > 0$. In other words, provided $b > 0$, the NLS equation (24) yields bright soliton solutions for all $p \in (0, 2\pi)$, and we find no threshold for the wavenumber p (that is, $p_{\min} = 0$). This case is considered in more detail in Section 4.

Using equations (24), (11) and (7) we determine an expression for the breather in the original displacement variable q_n. In the region above the curve corresponding to a particular wavenumber p in Figure 1, we expect to find bright soliton solutions to (25) of the form

$$F = A\,\mathrm{sech}\left(A\sqrt{\frac{Q}{2P}}Z\right)\exp\left(\mathrm{i}\frac{Q}{2}A^2T\right), \tag{29}$$

where the soliton amplitude A is a free parameter. Substituting (29) into the ansatz (11) gives the breather solution of (6) in terms of our $\phi_n(t)$ variables to second-order as

$$\phi_n(t) = 2\varepsilon A \text{ sech}\left[\varepsilon A\sqrt{\frac{Q}{2P}}\left(n+\cos\left(\frac{p}{2}\right)t\right)\right]\cos\left(\Omega t + pn\right)$$
$$+ 2a\varepsilon^2 A^2 \csc^2\left(\frac{p}{2}\right)\text{sech}^2\left[\varepsilon A\sqrt{\frac{Q}{2P}}\left(n+\cos\left(\frac{p}{2}\right)t\right)\right]$$
$$\times\left(\cos^2\left(\frac{p}{2}\right)\cos\left(2\Omega t + 2pn\right) - 1\right) + \mathcal{O}(\varepsilon^3), \tag{30}$$

where P and Q are defined in (25) above,

$$\Omega = 2\sin\left(p/2\right) + QA^2\varepsilon^2/2, \tag{31}$$

here, the combination εA is a single free parameter.

We use the leading-order solution for $\phi_n(t)$ in (30) to obtain an expression at leading-order for q_n, the original displacement variable. We assume that q_n is of the form

$$q_n(t) = 2\varepsilon A[\lambda\cos(\Omega t + pn) + \mu\sin(\Omega t + pn)]$$
$$\times \text{ sech}\left[\varepsilon A\sqrt{\frac{Q}{2P}}\left(n - vt\right)\right] + \mathcal{O}(\varepsilon^2), \tag{32}$$

where $v = -\cos(p/2)$ is the envelope velocity given in (19), and λ and μ are constants to be determined in terms of p, which is taken to be $\mathcal{O}(1)$.

We substitute (32) into the defining equation for ϕ_n (3), giving a second expression for $\phi_n(t)$ at leading order. Equating coefficients of corresponding terms in this and the leading-order expression for ϕ_n (30) yields the following simultaneous equations for λ and μ,

$$\lambda\cos p + \mu\sin p - \lambda = 1, \tag{33}$$
$$-\lambda\sin p + \mu\cos p - \mu = 0, \tag{34}$$

from which we find that $\lambda = -1/2$ and $\mu = (1/2)\cot(p/2)$. Hence overall we obtain an expression for the bright breather to leading-order

$$q_n(t) = -\varepsilon A\left[\cos(\Omega t + pn) - \cot\left(\frac{p}{2}\right)\sin(\Omega t + pn)\right]$$
$$\times\text{sech}\left[\varepsilon A\sqrt{\frac{Q}{2P}}\left(n - vt\right)\right] + \mathcal{O}(\varepsilon^2), \tag{35}$$

which is valid when $\varepsilon \ll 1$ and $p = \mathcal{O}(1)$. Note that equations (33) and (34) are ill-posed in the limit $p \to 0$.

Lastly in this section, we make a few remarks comparing the phase (or crest) velocity v_{crest} and the group (or envelope) velocity v_{envelope} of the carrier wave

of the breather solution (35). Clearly, $v_{\text{envelope}} = -\cos(p/2)$ is always less than unity. The crest velocity is given by $-\Omega/p$ and so from (31) this is also less than unity. For general p the two will differ, since $\sin\theta > \theta\cos\theta$ (for $0 < \theta < \pi$). In the limit of small p, the envelope and crest velocities $-\cos(p/2)$ and $-\Omega/p$ respectively are close, but $v_{\text{crest}} = -\Omega/p$ is always larger in magnitude when the $\mathcal{O}(\varepsilon^2)$ correction term is included. Thus there is no value of p for which $v_{\text{crest}} = v_{\text{envelope}}$.

Also, it is possible to use the existence criterion (26) (in particular, its rearrangement (28)) to find an upper bound for the envelope velocity v_{envelope}. Since the wavenumber p is restricted to the range $p_{\min} \leq p \leq \pi$, the breather velocity $v_{\text{envelope}} = -\cos(p/2)$ is restricted to the range

$$|v_{\text{envelope}}| < \sqrt{\frac{3b - 4a^2}{3b - 2a^2}}. \tag{36}$$

Thus for nonzero values of a, breather modes have a velocity which is bounded away from the speed of sound in the lattice.

We use the solution (35) to find a leading-order estimate for the total energy of the system, H, defined by (1). To leading order, H is given by

$$H \sim \frac{4\varepsilon A \sin(p/2)}{\sqrt{(6b - 4a^2)\sin^2(p/2) - 4a^2}} + \frac{p\pi \sin^2(p)\text{cosech}\left((p\pi/\varepsilon A)\sqrt{2P/Q}\right)}{(6b - 4a^2)\sin^2(p/2) - 4a^2}. \tag{37}$$

If we take all parameters to be $\mathcal{O}(1)$ except for $\varepsilon \ll 1$, then the second term on the right-hand side of (37) is exponentially small in ε. Hence overall, the energy H is an $\mathcal{O}(\varepsilon)$ quantity. In calculating the estimate for the energy H (37), we have used the expression for q_n given in (35). Since (35) is valid when $p = \mathcal{O}(1)$, it follows that the estimate for H (37) is also valid for this parameter regime.

2.4 The Toda lattice

We illustrate the results of our above analysis by referring to the Toda lattice, [29]. This lattice corresponds to $V(\phi) = \alpha[e^{-\beta\phi} + \beta\phi - 1]/\beta$ in (4), in which case $V'(\phi) = \alpha(1 - e^{-\beta\phi})$. Performing a Taylor expansion of $V(\phi)$ about $\phi = 0$, we find that $V'(\phi) \sim \alpha\beta[\phi - \beta\phi^2/2 + \beta^2\phi^3/6]$. Comparing this expansion with (5), we see that for the Toda lattice $a = -\alpha\beta^2/2$ and $b = \alpha\beta^3/6$. It follows that $3b = 2a^2$, and therefore the inequality (27) fails to hold for any p. We conclude that bright breathers can never exist in the Toda lattice. This nonexistence result is entirely consistent with the literature on Toda lattice (see [29]).

In the region below the curves in Figure 1, corresponding to wavenumbers p where (27) fails, we expect to find dark soliton solutions of the NLS equation. These solutions have the form $F(Z,T) = D(Z,T)\mathrm{e}^{\mathrm{i}\mu(Z,T)}$, where (see Chapter 4.5 of Remoissenet [20])

$$D(Z,T) = B\left[1 - m^2\,\mathrm{sech}^2\left(mB\sqrt{\frac{-Q}{2P}}Z\right)\right]^{\frac{1}{2}}, \tag{38}$$

$$\mu(Z,T) = \sqrt{\frac{-Q}{2P}}\left[\sqrt{1-m^2}BZ + \tan^{-1}\left\{\frac{m}{\sqrt{1-m^2}}\tanh\left(mB\sqrt{\frac{-Q}{2P}}Z\right)\right\}\right] - \frac{B^2Q}{2}(3-m^2)T. \tag{39}$$

Here, B is a free parameter (distinct from James' B-parameter discussed in Section 1) and m ($0 \leq m \leq 1$) is a parameter that controls the depth of the modulation of amplitude [20]. In this case, the overall solution of (6) in terms of the original variables to first order is $\phi_n(t) = 2\varepsilon D_n(t)\cos(\psi_n(t)) + \mathcal{O}(\varepsilon^2)$, where

$$D_n(t) = B\left[1 - m^2\,\mathrm{sech}^2\left\{mB\varepsilon\sqrt{\frac{-Q}{2P}}\left(n + \cos\left(\frac{p}{2}\right)t\right)\right\}\right]^{\frac{1}{2}}, \tag{40}$$

$$\begin{aligned}\psi_n(t) = {} & B\sqrt{\frac{-Q(1-m^2)}{2P}}\left[n + \cos\left(\frac{p}{2}\right)t\right] - \frac{B^2Q}{2}\varepsilon^2(3-m^2)t + 2\sin\left(\frac{p}{2}\right)t + pn \\ & + \sqrt{\frac{-Q}{2P}}\tan^{-1}\left[\frac{m}{\sqrt{1-m^2}}\tanh\left\{mB\sqrt{\frac{-Q}{2P}}\left(n + \cos\left(\frac{p}{2}\right)t\right)\right\}\right].\end{aligned} \tag{41}$$

These solutions have been observed previously, for example, by Flytzanis *et al.* [10].

3 Numerical results

In this section we numerically solve the equations for the FPU lattice (2). This infinite system of nonlinear coupled second-order ordinary differential equations is equivalent to the first-order system

$$\begin{aligned}\dot{q}_n &= p_n, \\ \dot{p}_n &= V'(q_{n+1} - q_n) - V'(q_n - q_{n-1}),\end{aligned} \tag{42}$$

where $p_n = \dot{q}_n$. We carry out the numerical simulation of the system using a fourth-order Runge-Kutta scheme coded in Fortran90. Our program solves the equations of motion for N particles where N is any natural number greater than or at least equal to three, but typically around 100. We note that the conservation of mechanical energy H (1) of the system can be used to check the validity of the numerical routines. The total energy H of the lattice is computed easily since it is a simple combination of the variables q_n and p_n returned by the numerical scheme. Also, we shall compare the numerically computed total energy with the asymptotic estimate given by (37).

Setting $t = 0$, we use our formula for $\phi_n(t)$ given in (30) to generate initial data for q_n,

$$q_n(t) = q_1(t) + \sum_{i=1}^{n-1} \phi_i(t) = \sum_{i=1}^{n-1} \phi_i(t), \tag{43}$$

where, for a breather initially located centrally in the lattice, we take $q_1 = 0$ following the comments on our choice of boundary conditions in (8). A similar equation holds for p_n. We note also that the constant $q_\infty = q_N(0)$.

We impose periodic boundary conditions by introducing fictitious particles at either end of the lattice, satisfying

$$\begin{aligned} q_{N+1}(t) &= q_1(t) + q_\infty, \quad \text{and} \quad q_0(t) = q_N(t) - q_\infty, \\ p_{N+1}(t) &= p_1(t), \qquad\quad \text{and} \quad p_0(t) = p_N(t). \end{aligned} \tag{44}$$

This has the consequence that breathers moving to the right- (left-) hand edge of the chain eventually reemerge from the left- (right-) hand edge.

We aim to verify the analytical results of Section 2, that is, whether the analysis correctly predicts the shape and velocity of stationary and moving waveforms in the chain. In particular, we will observe whether long-lived breather modes exist in the parameter regions where expected, that is, when a, b and p satisfy the inequality (26). Since the breather's exact position is hard to determine from plots of the breather profile, measuring the velocity of the breather accurately is difficult. We find that this is better achieved using a plot of the cell energy $e_n(t)$, where

$$e_n = \tfrac{1}{2} p_n^2 + V(q_{n+1} - q_n), \tag{45}$$

and $H = \sum_{n=1}^{N} e_n$ from (1). As we are dealing with a solitary waveform (that is, a localised disturbance whose amplitude decays to zero as $n \to \pm\infty$), the energy associated with the wave is also localised. Hence in order to track the position of the breather (and thus determine its velocity), we may equally use the location of the maximum value of e_n at each value of t.

Firstly, we present a simulation of a stationary breather ($p = \pi$). We choose

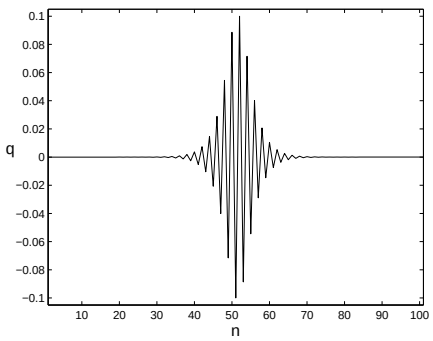

(a) Profile at $t = 0$.

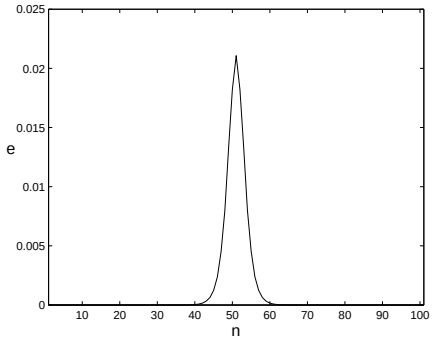

(b) Plot of e_n, $H = 0.1189$.

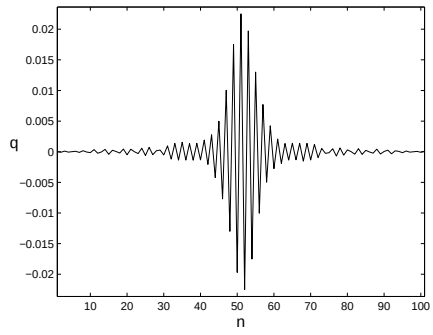

(c) Profile at $32.34T = 100$.

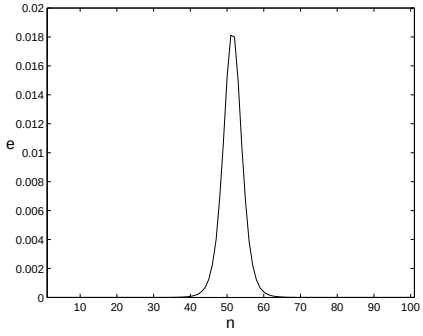

(d) Plot of e_n, $H = 0.1190$.

Fig. 2. Stationary breather, wavenumber $p = \pi$.

the remaining parameter values to be $a = 0.1$, $b = 2.0$, $N = 101$, $A = 1.0$ and $\varepsilon = 0.1$ which satisfy the existence criterion (26). The temporal frequency of the carrier wave is $\Omega = 2.2098$, and hence it follows that the period of oscillation is $T = 2\pi/\Omega = 3.0955$. The breather is initially located at the centre of the chain (as is the case for all of our simulations), and is shown in Figure 2 (a). The profile of the breather is also shown at a later time, $t = 32.31T = 100$ in Figure 2 (c). At both times, a plot of the cell energy is also given. From the energy plots, it is clear that after 100 seconds, the breather has not spread or distorted significantly. We have also included the numerically computed values of the total energy H. After 100 seconds, we see that the change in H is negligible, with $\Delta H/H = 0.00084$. The asymptotic estimate of H given by (37) is 0.1159, which is a little lower than the numerically obtained values. This is to be expected, since in deriving (37), we ignored $\mathcal{O}(\varepsilon^2)$ terms, which make a small contribution. In Figure 3, we have shown a montage of snapshots of the breather at times $t = 0$, $5T$, $10T$, $15T$, $20T$ and $25T$. From this, we

see that the breather does not spread or diminish in amplitude over this time interval.

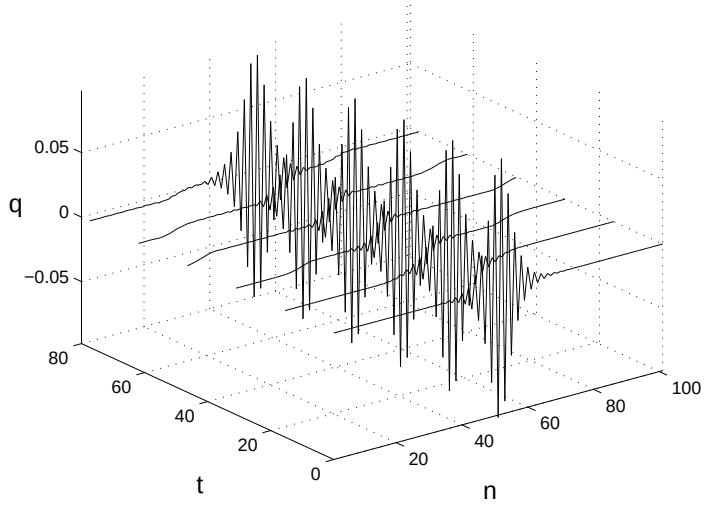

Fig. 3. Snapshots of the stationary breather at times $t = 0$, $5T$, $10T$, $15T$, $20T$ and $25T$, $T = 3.0955$.

We now present a simulation of a moving breather. For this, we set wavenumber $p = \pi/2$, for which $v = -\cos(p/2) = -1/\sqrt{2}$ units per second. The remaining parameters are chosen as follows: $a = 0.1$, $b = 2.0$, $N = 101$, $A = 1.0$ and $\varepsilon = 0.1$, which satisfy the existence inequality (26). In this case, the breather frequency is $\Omega = 1.4353$, and so the oscillation period is $T = 4.3779$. We do not show the initial profile of the breather this time, though we have shown the profile at times $t = 50$ and $t = 91.76$ in Figures 4 (a) and 4 (c) respectively. In the first of these, we see that the breather has moved to the left and has almost reached the left-hand edge of the chain. A little while later, it disappears from this side and reappears from the right-hand edge (see Figure 4 (c)). This is due to the periodic boundary conditions. By calculating e_n (45) and plotting it against n, we find, from Figure 4 (d), that the average velocity of the breather is -0.703 units per second. Hence the percentage difference between the analytical and numerical velocities is -0.58%. In Figure 4, we have included the numerically computed values of the energy H. Again, we see that there is only a tiny change in the computed value over the entire duration, with $\Delta H/H = -0.00083$. There is also a close match with the asymptotic estimate for H, which turns out to be 0.1161. In Figure 5, we show the breather at various stages of its motion as it travels leftwards through the chain. The last snapshot at $t = 142.86$ shows the breather as it has just completed one whole circuit and returned to its initial position. In this example we observe a small amount of energy escape from the front of the breather.

We also use our numerical scheme to further test the existence inequality (26).

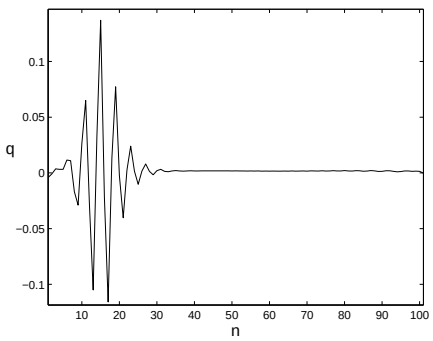

(a) Profile at $t = 50$.

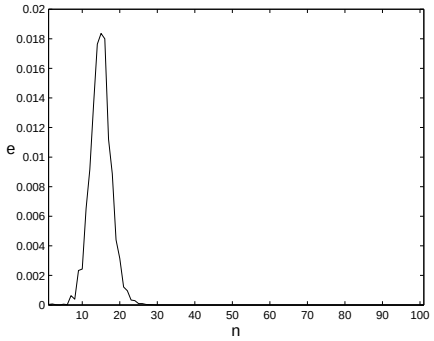

(b) Plot of e_n, $H = 0.1199$.

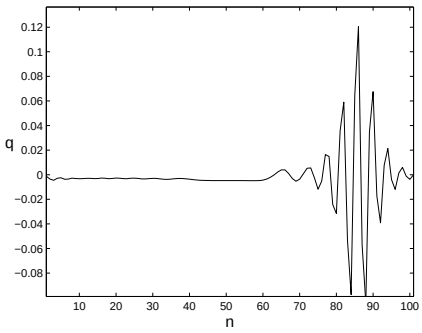

(c) Profile at $t = 91.76$.

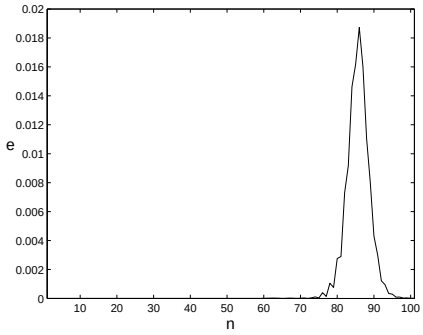

(d) Plot of e_n, $H = 0.1198$.

Fig. 4. Moving breather, wavenumber $p = \pi/2$.

In Section 2.3, we showed that a necessary condition for breather existence in the FPU chain is that $3b > 4a^2$. In addition to this, for $a \neq 0$, the wavenumber p must be greater than the minimum wavenumber $p_{\min}$ given by (28). It is natural to question what happens as wavenumber $p \to p_{\min}^{+}$, that is, when the existence condition (26) is only just satisfied. We now show that the breather becomes wider as p approaches this threshold.

In order to quantify this, we introduce the notion of a breather's width. If we consider the envelope of the breather given by (35), the envelope half-width L_{hw} is measured at half the maximum amplitude of the breather, which is εA. In other words, L_{hw} satisfies $2\varepsilon A \operatorname{sech}(\varepsilon A L_{\text{hw}} \sqrt{Q/2P}) = \varepsilon A$

$$L_{\text{hw}} = \frac{1}{\varepsilon A} \sqrt{\frac{2P}{Q}} \operatorname{sech}^{-1}\left(\frac{1}{2}\right). \tag{46}$$

The full width of the breather L_{fw} is simply twice the half-width, that is,

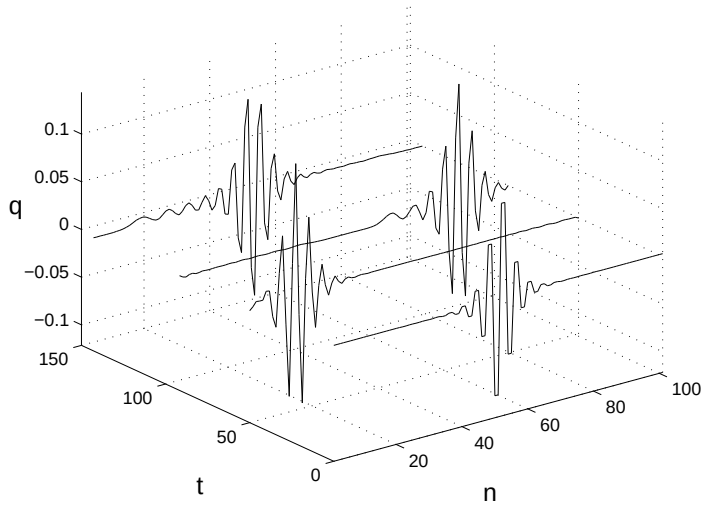

Fig. 5. Snapshots of the moving breather at times $t = 0$, 50, 91.76 and 142.86.

$L_{\rm fw} = 2L_{\rm hw}$. Rewriting the term $Q/2P$ as $6b - 4a^2 - 4a^2\mathrm{cosec}^2\,(p/2)$, we see that $\sqrt{(Q/2P)}$ decreases to zero as p decreases to $p_{\rm min}$, hence the width of the breather $L_{\rm fw}$ increases without bound as $p \to p^+_{\rm min}$. If we choose $a = 1$ and $b = 2$, then from (28) it follows that $p_{\rm min} = \pi/2$. In Figure 6, we show the initial profiles of two breathers which correspond to two different wavenumbers. For both, we have set $a = 1.0$, $b = 2.0$, $N = 101$, $A = 1.0$ and $\varepsilon = 0.1$. In Figure 6 (a), we set $p = \pi$, and in Figure 6 (b) we set $p = 1.7$, which is much closer to the threshold value of $\pi/2 \approx 1.57$. As expected, the breather is much wider for $p = 1.7$ than for $p = \pi$. Using the definition (46), for $p = \pi$ we find that $L_{\rm fw} = 13.17$, while for $p = 1.7$ we find $L_{\rm fw} = 27.57$, which is more than twice as wide.

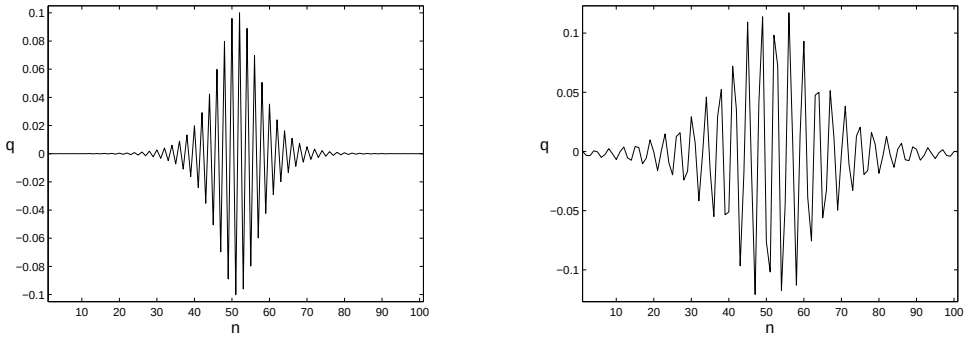

(a) $p = \pi$. (b) $p = 1.7$.

Fig. 6. Widening of breather profile as $p \to p^+_{\rm min} = \pi/2$.

4 The limit of small wavenumber: $p \to 0$

4.1 Preliminary results

In this section we show that the FPU lattice can support waveforms more complex than bright or dark breathers or travelling kinks. These more complex waveforms arise when we consider small wavenumbers p (we quantify what we mean by "small" more precisely in Section 4.3). Since we consider arbitrarily small wavenumbers p, most of this section is concerned with the case of the quartic lattice, that is, $b > 0$, $a = 0$ (this follows from the comments after equation (28)). However, in Section 4.2, we note the behaviour of kinks in the lattice with cubic nonlinearity in the potential energy, (that is, $a > 0$, $b = 0$). This is to demonstrate that behaviour in the lattice with quartic potential is quite distinct and unusual when compared with that observed in the lattice with a cubic potential.

Firstly, we show that for the quartic lattice ($a = 0$, $b > 0$), the solution (30) reduces to a kink in the limit $p \to 0$. Considering only the leading-order expansion for $\phi_n(t)$, we note that as $p \to 0$, $\cos(p/2) \to 1$, and also from (31), $\Omega \to 0$ and hence $\cos(\Omega t + pn) \to 1$. Overall, when $p \ll \varepsilon \ll 1$, we have

$$\phi_n(t) = 2\varepsilon A \operatorname{sech}\left[A\sqrt{\frac{Q}{2P}}(\varepsilon n + \varepsilon t)\right] + \mathcal{O}(\varepsilon^3). \tag{47}$$

Since ϕ_n is slowly varying in n, (7) can be replaced by $q_n = \int_\infty^n \phi_k \, \mathrm{d}k$, and so (47) gives

$$q_n(t) = 4\sqrt{\frac{2P}{Q}} \tan^{-1}\left[\exp(\varepsilon A\sqrt{\frac{Q}{2P}}(n+t))\right], \tag{48}$$

which describes a kink travelling leftwards through the chain whose speed, to leading order, is unity. Using (48) and (8), we find that the amplitude of the kink is given by

$$q_\infty = 2\pi\sqrt{\frac{2P}{Q}} = \frac{2\pi}{\sqrt{6b}}. \tag{49}$$

So in the limit $p \to 0$, the bright breather solution given in (30) reduces to q_n as given in (48) which describes a travelling kink.

We use our numerical simulation to test whether kinks are observed in the lattice for very small wavenumbers p. We run our simulation for the parameter values $p = 0.01$, $a = 0.0$, $b = 2.0$, $N = 101$, $A = 1.0$ and $\varepsilon = 0.1$. In Figure 7, we show the kink at intervals of 10 seconds as it moves leftwards through the chain. For instance, by the time $t = 30$, we see that the kink is close to the left-hand edge of the chain. From (19), for very small wavenumbers we expect the speed of the kink to be very close to unity. Using the method described in

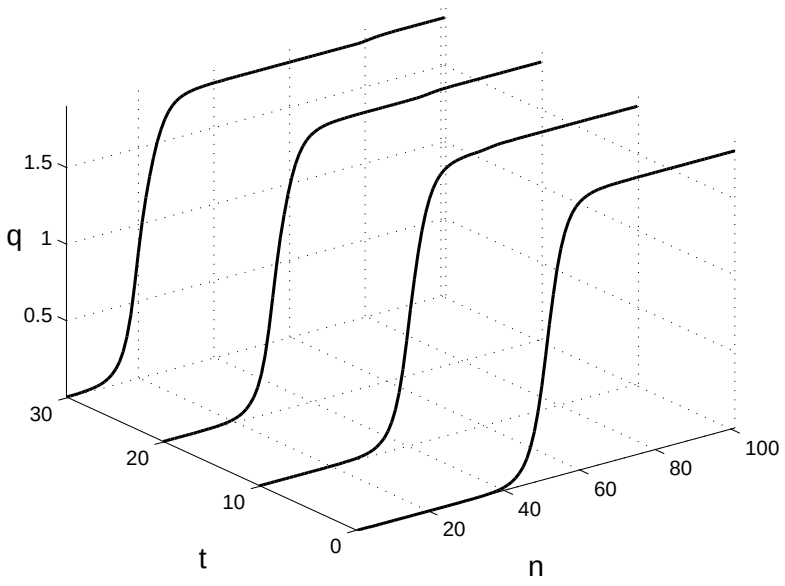

Fig. 7. Kink for wavenumber $p \to 0$: $a = 0$, $b = 2$ and $p = 0.01$.

Section 3, we measure the velocity of the kink and find it to be -1.03 units per second. Hence there is a 3% difference between the theoretical and observed values of -1 and -1.03 units per second respectively. We also measure the height of the kink to be 1.8, which is in close agreement (a difference of -0.6%) with the calculated value of 1.81 given by (49).

The calculation presented in (49) gives the amplitude of the kink for the small wavenumber limit $p \to 0$. Later in Section 4.3 we will present details of the calculation of q_∞ for the more general case $p = \mathcal{O}(\varepsilon)$. Firstly, we summarise some known properties of kinks in the FPU lattice.

4.2 Travelling kinks in the classical continuum limit

In this section, we consider the FPU lattice with either a cubic or a quartic potential. We saw in the previous section that for very small wavenumbers ($p \ll \varepsilon \ll 1$), the breather solution of the quartic FPU lattice reduces to a travelling wave which has the form of a kink. However, travelling kink solutions can be determined directly from the equations of motion (6) provided the parameters a and b are chosen appropriately. Since the discrete lattice equations are not solvable exactly, we approximate them using continuum approximations (in which the discrete index n in (6) is replaced by a continuous variable). We use results from Collins [6], Collins & Rice [7], Rosenau [21, 22] and Wattis [31]. We analyse kink solutions in the two special cases of lattices

with a symmetric quartic potential ($a = 0, b \neq 0$) and an asymmetric cubic potential ($a \neq 0, b = 0$).

4.2.1 The lattice with a cubic potential ($a \neq 0$, $b = 0$)

In the simplest approximation (that is, the standard continuum approximation) the lattice dynamics (6) are approximated by the partial differential equation

$$\phi_{tt} = \phi_{xx} + \tfrac{1}{12}\phi_{xxxx} + a(\phi^2)_{xx}, \tag{50}$$

which has a travelling wave solution in the form of a pulse for ϕ

$$\phi_{2s}(z) = \frac{3(c^2-1)}{2a}\text{sech}^2\left(z\sqrt{3(c^2-1)}\right), \tag{51}$$

where $z = x - ct$, and c is the velocity of the travelling wave. This gives rise to a travelling kink in the variable q which has amplitude and energy given by

$$q_\infty^{(2s)} = \frac{\sqrt{3(c^2-1)}}{a}, \qquad H_{2s} = \frac{\sqrt{3}(c^2-1)^{3/2}(9c^2+1)}{10a^2}. \tag{52}$$

Equation (50) is not a good approximation to the kinetics of the lattice equation (6) due to it being ill-posed; the dispersion relation for (57) is

$$\omega^2 = p^2 - \tfrac{1}{12}p^4, \tag{53}$$

which is a poor approximation to (17). For larger wavenumbers ($p > 2\sqrt{3}$) equation (53) gives rise to imaginary values for ω which correspond to unphysical, exponentially-growing, waves, whereas (17) gives $\omega \in \mathbb{R}$ for all wavenumbers p.

If we use an improved continuum approximation, then we obtain a different PDE approximation of (6), namely

$$\phi_{tt} = \phi_{xx} + \tfrac{1}{12}\phi_{xxtt} + a(\phi^2)_{xx}. \tag{54}$$

This partial differential equation is well-posed, having the dispersion relation $\omega^2 = p^2/(1 + \frac{1}{12}p^2)$, which gives real values of ω for all wavenumbers, p. Equation (54) supports a travelling pulse for ϕ of the form

$$\phi_{2i}(z) = \frac{3(c^2-1)}{2a}\text{sech}^2\left(\frac{z\sqrt{3(c^2-1)}}{c}\right). \tag{55}$$

From this, we find slightly more accurate estimates for the kink-amplitude and energy,

$$q_\infty^{(2i)} = \frac{c\sqrt{3(c^2-1)}}{a}, \qquad H_{2i} = \frac{c^3\sqrt{3}(c^2-1)^{3/2}}{a^2}. \tag{56}$$

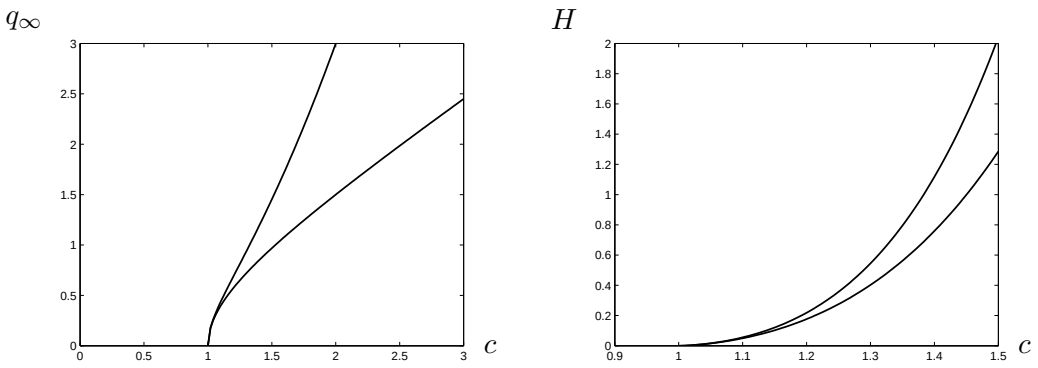

(a) Kink height q_∞.

(b) Kink energy H.

Fig. 8. Height and energy of kinks in a chain with cubic potential, ($a = 2$, $b = 0$) (see equations (52) and (56)).

We note that these have the same behaviour as $c \to 1$ as those generated from the standard continuum approximation. In particular for both, we observe that as $c \to 1^+$, $q_\infty \to 0^+$ and $H \to 0^+$. Also both approximations yield similar behaviour for large values of c. That is, as $c \to \infty$ we have $q_\infty \to \infty$ and $H \to \infty$. The properties for both the standard and improved continuum approximations are illustrated in Figure 8, which shows plots of the kink-amplitude q_∞ in Figure 8 (a) and the energy H in Figure 8 (b), against the velocity c. In both plots, the upper curve corresponds to the improved continuum approximation. This behaviour is as expected and contrasts with the lattice with a quartic term and no cubic term in the interaction potential as we shall now see.

4.2.2 The lattice with a quartic potential ($a = 0$, $b > 0$)

In this case, the standard continuum approximation of (6) is

$$\phi_{tt} = \phi_{xx} + \tfrac{1}{12}\phi_{xxxx} + b(\phi^3)_{xx}, \tag{57}$$

which is again an ill-posed partial differential equation. However, a travelling-wave solution can still be found from it, which, in the ϕ variables, gives rise to the pulse solution

$$\phi_{3s}(z) = \sqrt{\frac{2(c^2-1)}{b}}\operatorname{sech}\left(2z\sqrt{3(c^2-1)}\right). \tag{58}$$

Following the transformation back to the q variables we again have a travelling kink with kink-amplitude and energy

$$q_\infty^{(3s)} = \frac{\pi}{\sqrt{6b}}, \qquad H_{3s} = \frac{(5c^2+1)}{3b}\sqrt{\frac{c^2-1}{3}}. \tag{59}$$

Note that H_{3s} has the expected behaviour of $H \to \infty$ as $c \to \infty$ and $H \to 0^+$ as $c \to 1^+$. However, $q_\infty^{(3s)}$ does not share these properties as it is independent of the speed c. Partly this is due to the expression (58) being a poor approximation to the waveform of the travelling pulse solution.

In place of (57) an improved approximation to (6) is the well-posed partial differential equation

$$\phi_{tt} = \phi_{xx} + \tfrac{1}{12}\phi_{xxtt} + b(\phi^3)_{xx}, \tag{60}$$

which supports a pulse solution of form

$$\phi_{3i}(z) = \sqrt{\frac{2(c^2-1)}{b}}\operatorname{sech}\left(\frac{2z\sqrt{3(c^2-1)}}{c}\right). \tag{61}$$

The solutions (58) and (61) show that travelling kinks are expected to be supersonic ($c > 1$) as the kink illustrated in Figure 7 (end of Section 4.1) was found to be. Integrating (58) or (61) with respect to z shows the kink $q(z)$ to have the same form as noted in (48), namely $A\tan^{-1}\mathrm{e}^{\lambda z}$ for some A, λ. From (61), we find more accurate expressions for the kink-amplitude and energy than those in (59), namely

$$q_\infty^{(3i)} = \frac{\pi c}{\sqrt{6b}}, \qquad H_{3i} = \frac{2c^3}{b}\sqrt{\frac{c^2-1}{3}}. \tag{62}$$

In (62), we note that H_{3i} shares similar properties with H_{3s}. However, $q_\infty^{(3i)}$ now satisfies the condition $q_\infty^{(3i)} \to \infty$ as $c \to \infty$, but as $c \to 1^+$, $q_\infty^{(3i)} \to \pi/\sqrt{6b} \neq 0$. The amplitude q_∞ and energy H of the kink solutions for the quartic potential is plotted in Figure 9. Again, the upper curve corresponds to the improved continuum approximation.

For quartic systems which are initiated with boundary data of the form

$$\begin{aligned} q_n &\to q_\infty \quad \text{as} \quad n \to \infty \\ q_n &\to 0 \quad\;\; \text{as} \quad n \to -\infty, \end{aligned} \tag{63}$$

with $q_\infty > \pi/\sqrt{6b}$ we might expect the large-time evolution of the system to be governed by a kink of amplitude q_∞, which travels at a speed approximately equal to $q_\infty\sqrt{6b}/\pi$. However, for a system which is initiated with boundary

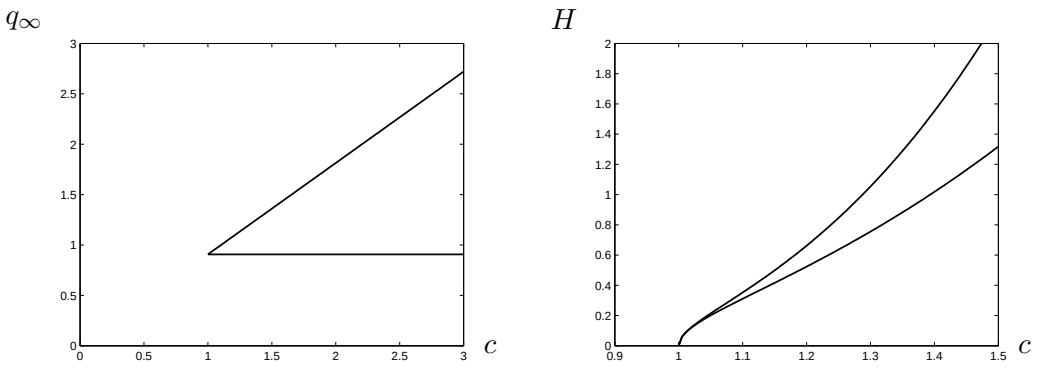

(a) Kink height q_∞.

(b) Kink energy H.

Fig. 9. Height and energy of kinks in a chain with quartic potential, ($a = 0$, $b = 2$) (see equations (59) and (62)).

data of the form (63) with $q_\infty < \pi/\sqrt{6b}$, there is no travelling kink of this amplitude which can be an attractor for the large-time dynamics. This leaves the open problem of what (if any) coherent structures would be observed at large times in a system with such initial data. For convenience, we will hereupon define $q_\infty^{(c)} := \pi/\sqrt{6b}$.

4.3 Combinations of breathers and kinks in the FPU chain

We return to the moving breather modes for which asymptotic approximations were calculated in Section 2.3. In this section, we are concerned with small wavenumbers, ($p \ll 1$). In order for our method to generate a moving breather mode with arbitrarily small wavenumber p, we confine attention to the quartic FPU lattice ($a = 0$, $b > 0$) throughout this section.

We show that, in the $q_n(t)$ variables, the moving breather mode combines both kink and breather elements, and we analyse the relative importance of each component. From (30), the amplitude of the breather component is $\mathcal{O}(\varepsilon)$. The size of the kink component q_∞ is given by the sum in (8). We are unable to find an exact expression for q_∞ for general small p, but we can find q_∞ to leading order. We will see that q_∞ depends upon the relative sizes of p and ε. Note from (25) that $\sqrt{Q/2P} = \sqrt{6b}$ independent of p, since $a = 0$.

From the definition of q_∞, (8), and the solution for ϕ_n (30), we have

$$q_\infty = \sum_{n=-\infty}^{\infty} \phi_n \sim \sum_{n=-\infty}^{\infty} \frac{2\varepsilon A \cos(pn + \Omega t - s)}{\cosh[\varepsilon A\sqrt{6b}(n - n_0 - vt)]}, \tag{64}$$

where n_0 and s represent arbitrary shifts in the waveform of the envelope and the phase of the carrier wave. Replacing the sum by an integral (since the summand is slowly varying in n due to $\varepsilon \ll 1$ and $p \ll 1$) we obtain

$$q_\infty \sim \frac{2\pi}{\sqrt{6b}} \operatorname{sech}\left(\frac{\pi p}{2\varepsilon A\sqrt{6b}}\right) \cos\left((pn_0 - s) + (pv + \Omega)t\right). \tag{65}$$

using formula 3.981.3 of Gradshteyn & Ryzhik [14]. The estimate (65) for q_∞ appears to time-dependent, though it evolves over an extremely long time-scale, since for small p and small ε, we have

$$pv + \Omega \sim \tfrac{1}{12} p\left(p^2 + 9b\varepsilon^2 A^2\right). \tag{66}$$

by (31) and $v = -\cos(p/2)$. Thus if, for example, $p = \mathcal{O}(\varepsilon)$ then q_∞ evolves over a timescale of $t = \mathcal{O}(\varepsilon^{-3})$. If we are concerned with the evolution over timescales up to $\mathcal{O}(\varepsilon^{-2})$, then (65) can be treated as time-independent.

Clearly from (65), the size of q_∞ depends upon the relative magnitudes of p and ε. For instance, if $p \gg \varepsilon$ then the amplitude of the kink is small. Indeed as p approaches $\mathcal{O}(1)$, the amplitude of the kink becomes exponentially small in ε, and hence in this regime, the amplitude of the breather dominates that of the kink. However, if $p \ll \varepsilon$ or $p \sim \varepsilon$, then the amplitude of the kink is $\mathcal{O}(1)$ and this dominates the breather (which has amplitude $\mathcal{O}(\varepsilon)$ for all p).

We also note from (65) that: (i) the amplitude q_∞ is maximised when $s = pn_0$, that is, when the maximum of the envelope $n = n_0$ coincides with a maximum of the carrier wave $\cos(pn + \Omega t - s)$; (ii) there is a one-parameter family of breathers with accompanying zero kink-amplitude, that is, for $s = pn_0 + \pi/2$ the amplitude of the kink component vanishes, leaving a pure breather.

We mention in passing that in the limit $p \to 0$, (65) agrees with the preliminary result (49), both giving a kink height of $2\pi/\sqrt{6b}$. We show a plot of q_∞ given by (65) against wavenumber p for two different values of ε in Figure 10. The upper curve corresponds to $\varepsilon = 0.025$, and the lower to $\varepsilon = 0.01$. The remaining parameters in (65) are set as $n_0 = 0$, $s = 0$, $A = 1$ and $b = 2$ in both plots. Note that the two curves have the same value in the limit $p \to 0$, that is, $2\pi/\sqrt{6b} \approx 1.81$.

There is an intermediate regime in which $p \ll 1$ and $\varepsilon \ll 1$ in which kink and breather have comparable amplitudes. As we reduce p, it is at this magnitude that coupled breather-kinks (which we term *breathing-kinks* for convenience) become most apparent. To determine the magnitude of this wavenumber, we first note that the amplitude of the breather is ε for all p. To find the value of p for which the amplitudes of the kink (given by (65)) and breather are

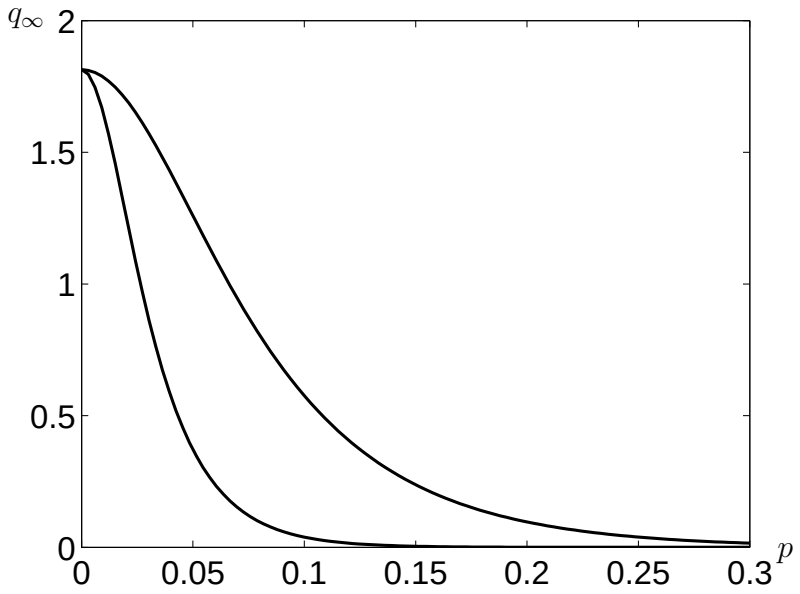

Fig. 10. Plot of q_∞ given by (65) against wavenumber p. The upper and lower curves correspond to $\varepsilon = 0.025$ and $\varepsilon = 0.01$ respectively.

similar, we solve

$$q_\infty \sim \frac{4\pi}{\sqrt{6b}} \exp\left(\frac{-\pi p}{2\varepsilon A\sqrt{6b}}\right) \sim \varepsilon, \tag{67}$$

from which we deduce that

$$p \sim \frac{2\varepsilon A\sqrt{6b}}{\pi} \log\left(\frac{4\pi}{\varepsilon\sqrt{6b}}\right). \tag{68}$$

Hence for $p = \mathcal{O}(\varepsilon \log(1/\varepsilon))$, the breather and kink components have comparable amplitudes, and we have $\varepsilon \ll p \ll 1$.

The most natural range to study further is $p = \mathcal{O}(\varepsilon)$ which differs only slightly from (68). We calculate the energy H to leading order. Since $p \sim \varepsilon$, we write $p = \kappa\varepsilon$, where $\kappa = \mathcal{O}(1)$. The total energy, H, is given by (1). To simplify the ensuing calculations, we use θ and ψ to denote $pn + \Omega t$ and $\varepsilon A\sqrt{Q/2P}(n + \cos(p/2)t)$ respectively. After differentiating $q_n(t)$ (35) with respect to t, and substituting for $\dot{q}_n$ and ϕ_n in (1), we have

$$H \sim \sum_{n=-\infty}^{\infty} \tfrac{1}{2}\varepsilon^2 A^2 \mathrm{sech}^2\psi \left\{4\cos^2\theta + \Omega^2\left[\sin\theta + \cot\left(\frac{p}{2}\right)\cos\theta\right]^2\right\}. \tag{69}$$

Since $p = \kappa\varepsilon$, it follows that $\cot(p/2) \sim 2/\varepsilon\kappa$ and that $\Omega \sim 2\sin(p/2) \sim \varepsilon\kappa$. Also, we have that $\psi = \varepsilon A\sqrt{6b}(n + t)$ and $\theta = \varepsilon\kappa(n + t) = \kappa\psi/A\sqrt{6b}$. Thus,

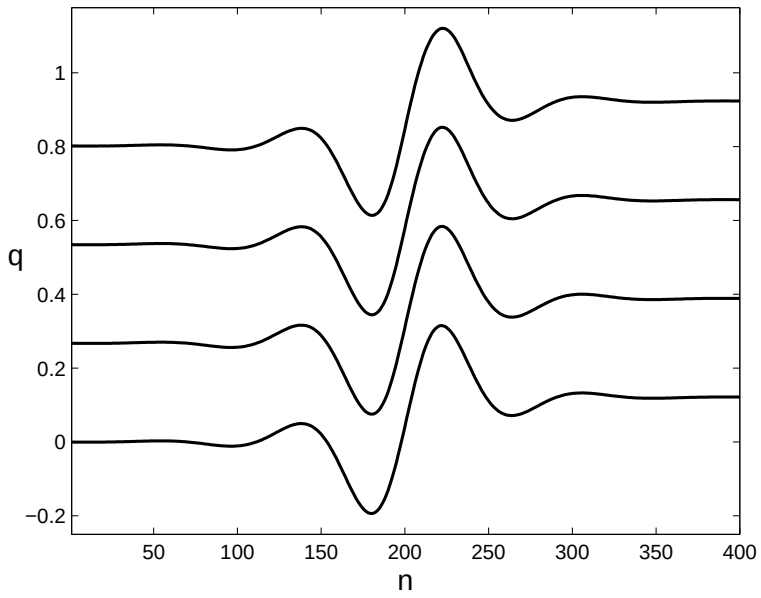

Fig. 11. Breathing-kink with $q_\infty < q_\infty^{(c)}$ displayed every 800 time units from $t = 0$ to $t = 2400$.

retaining terms to leading order only, we find that (69) becomes

$$H \sim \frac{4\varepsilon A}{\sqrt{6b}} \int_{-\infty}^{\infty} \cos^2\left(\frac{\kappa\psi}{A\sqrt{6b}}\right) \operatorname{sech}^2\psi \, \mathrm{d}\psi, \tag{70}$$

where the sum in (69) has been replaced by an integral. Applying formula 3.982.1 of Gradshteyn & Ryzhik [14], we then have an estimate for the total energy when the wavenumber $p = \mathcal{O}(\varepsilon)$ of

$$H \sim \frac{4\varepsilon A}{\sqrt{6b}} + \frac{2\kappa\varepsilon\pi}{3b \sinh\left(\kappa/A\sqrt{6b}\right)} = \mathcal{O}(\varepsilon). \tag{71}$$

4.4 Numerical results

We have run numerical simulations of the system with small wavenumbers to investigate the behaviour of breathing kinks. To illustrate their stability we present the results of a lattice of size $N = 400$, simulated for a time of $T = 2400$ time units. The nonlinear interaction potential has $a = 0$, $b = 2$ and we set $\varepsilon = 0.01$, $p = 0.075$ and $A = 1$. The results are displayed in Figure 11.

A snapshot is shown every other time that the wave passes the centre of the lattice (since the lattice has size $N = 400$, and the velocity of the wave is close to unity, this occurs approximately every 800 seconds). The wave

moves to the left, so that every circuit, the lattice site displacements $q_n(t)$ register a raise of $q_\infty \approx 0.12$ (recall that we are using periodic boundary conditions). Whilst each individual snapshot of the wave in Figure 11 clearly shows both oscillatory (breather) and kink characteristics of the waveform, from the montage of results, the wave actually appears to have the form of a travelling wave. This is because for small p, the phase velocity ($\omega/p = 1 - p^2/24 + \mathcal{O}(p^4)$) and the envelope velocity ($v = 1 - p^2/8 + \mathcal{O}(p^4)$) are almost identical. Any internal breathing in the wave occurs on a timescale of $\mathcal{O}(1/p^2)$ which is too long to observe in the simulations we have carried out. To observe a difference in velocities, it would be necessary to observe a shift of, say, five lattice spacings, which takes a time of $\sim 5/\Delta v = 60/p^2 \approx 10^4$ with the parameter values as in Figure 11. The simulation illustrated above, however, confirms that the mode is extremely long-lived and satisfies boundary conditions which are inaccessible to traditional kink travelling wave solutions of FPU lattices with quartic interaction potentials (see the closing comments of Section 4.2). The leading-order estimate for q_∞ given by (65) for the parameter values used in this simulation gives a value of 0.1208, which is very close to the measured value 0.12. This value is considerably smaller than the minimum amplitude of classical monotone kinks which is $q_\infty^{(c)} = \pi/\sqrt{6b} \approx 0.907$.

Whilst the above example shows that breathing-kinks exist with $q_\infty < q_\infty^{(c)}$, that is, in the range of amplitudes where traditional travelling kinks are forbidden (see Section 4.2), we now examine breathing-kinks in the range $q_\infty^{(c)} < q_\infty < 2q_\infty^{(c)}$. In this latter parameter range, both breathing-kinks and traditional (monotone) kinks exist. We therefore investigate numerically the stability of breathing-kinks, since for example, it is possible that the mode could decompose into a supersonic ($c > 1$) classical (monotone) kink and a subsonic ($c < 1$) classical breather. Figure 12 shows the results of such a simulation. For this, we have set $a = 0$, $b = 2$, $\varepsilon = 0.01$, $A = 1$ and $p = 0.025$. Of course, since this corresponds to an even smaller wavenumber than the previous example, the expected time for breathing to be observed is once again beyond a straightforward numerical simulation (requiring an integration in excess of $t = 10^5$). The wave moves to the left, and is depicted in Figure 12 at times $t = 0$ (central curve), 550 (right curve) and 1250 (left curve) seconds. During these intervals, it makes a complete circuit (or thereabouts) of the lattice. The vertical displacement is adjusted modulo q_∞ to allow easy comparison of the waveform. We see that the mode is a travelling wave of permanent form over this timescale. The observed value of q_∞ is approximately 1.05, which is in excellent agreement with the theoretical value of 1.058 given by (65).

In this section we have demonstrated that in the quartic FPU lattice, traditional kink travelling wave solutions have an amplitude of $q_\infty > q_\infty^{(c)} := \pi/\sqrt{6b}$ (see the right-hand side of Figure 13), and travel at supersonic speeds, (c > 1). We have then shown that for small wavenumbers p, our breather modes give

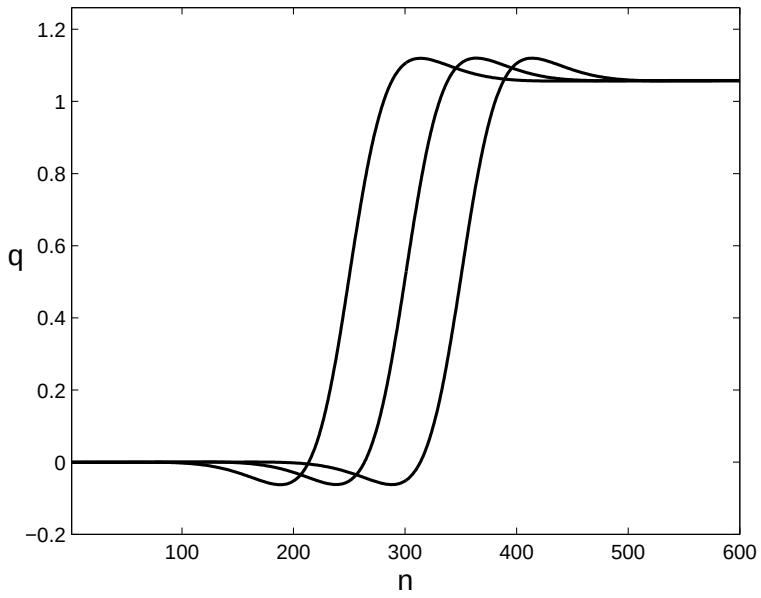

Fig. 12. Breathing-kink with $q_\infty^{(c)} < q_\infty < 2q_\infty^{(c)}$ displayed approximately every 600 seconds.

rise to waves which share features of both travelling kinks and breathers and, in particular, exhibit kink amplitudes in the range $0 < q_\infty < 2q_\infty^{(c)}$ (see the left-hand side of Figure 13). These combined breathing-kinks travel subsonically (that is, $c < 1$).

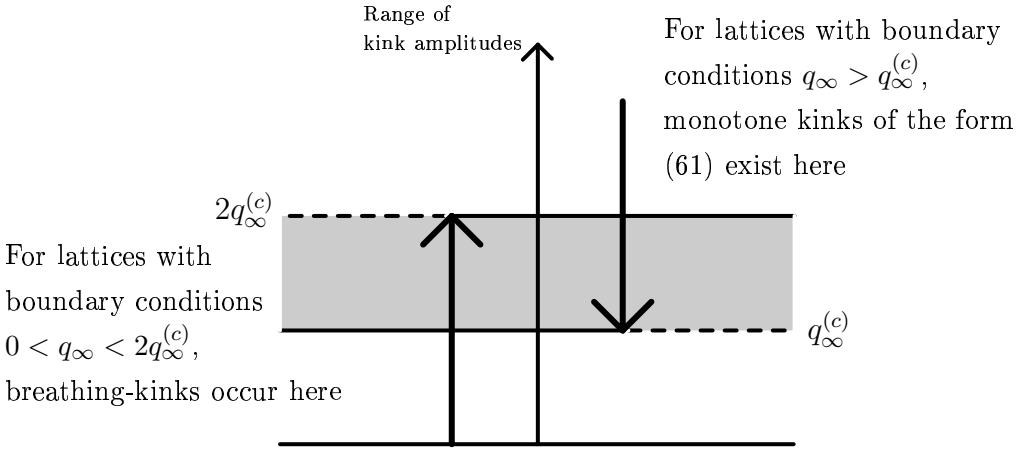

Fig. 13. Types of waveform which may occur in the quartic FPU chain, depending upon the size of q_∞. Note that $q_\infty^{(c)} := \pi/\sqrt{6b}$.

Thus for lattices with boundary conditions (63) in the range $0 < q_\infty < q_\infty^{(c)}$ we have a waveform which may be observed in the large time limit. Also for lattices with boundary conditions in the range $q_\infty^{(c)} < q_\infty < 2q_\infty^{(c)}$ there is now the possibility of two types of kink solution – namely the traditional monotone

travelling wave, and the breathing-kink. This corresponds to the shaded band in Figure 13. Equation (65) gives an asymptotic estimate for the relationship between q_∞ and wavenumber p ($p \ll 1$) and phase shifts n_0 and s which any breathing-kink must satisfy; this relationship is illustrated in Figure 10.

5 Discussion

In this paper, using asymptotic analysis, we have reduced the equations of motion for an FPU lattice with a polynomial potential V to a nonlinear Schrödinger (NLS) equation. Requiring the NLS equation to have localised soliton solutions leads to the identification of a region of parameter space in which the FPU lattice can support breathers. This is a region in which the coefficient of the quartic nonlinearity must exceed some multiple of the square of the cubic coefficient. There is then a range of wavenumbers for which breather modes exist (see inequality (26)). We have also given a full description of the parts of (a, b, p) parameter space where localised modes involved in energy transport exist, and provided a physical justification for the inequality proven by James [17] for stationary breathers.

Our systematic derivation of equations down to $\mathcal{O}(\varepsilon^4)$ yields the first correction term as well as the leading order behaviour. The calculation of the breather shape given by (30) is technically cumbersome since equations from $\mathcal{O}(\varepsilon)$ up to $\mathcal{O}(\varepsilon^4)$ must be solved just to obtain the leading order $\mathcal{O}(\varepsilon)$ solution for the breather. Numerical simulations in Section 3 verified the inequality (26), as we observed bright breather solutions for appropriate parameter values. We have also noted that when there are both cubic and quartic anharmonicities present in the interaction potential, the bright breather solution ceases to exist as the wavenumber is reduced to some finite positive value. This is due to the width of the envelope function diverging at some critical wave number given by (28). This gives rise to a maximum velocity for breathers, that is, rather than existing at all speeds from zero up to the speed of sound, there is an upper limit on the speed, given by equation (36).

In Section 4, by considering small wavenumbers, we found waveforms supported by the lattice that are more complex than breathers. We have termed these "breathing-kinks" because although they appear to have the form of travelling waves, a snapshot has the appearance of a combination of a breather and a kink. We have shown that the symmetric FPU lattice (where the potential has only a quartic nonlinearity, and no cubic component) supports traditional monotone travelling kinks only above a critical amplitude, $q_\infty^{(c)}$, whereas breathing-kinks have kink amplitudes in the range $0 < q_\infty < 2q_\infty^{(c)}$. The type of waveform exhibited ultimately is determined by the order of magnitude of q_∞, which depends in turn upon the relative magnitudes of the wavenumber

p and breather amplitude ε as well as temporal and spatial phase-shifts s and n_0. We found that in the limit $p \to 0$, the kink dominates and the breather component has vanishingly small amplitude. For $\mathcal{O}(1)$ wavenumbers, the amplitude of the breather dominates that of the kink. The two components have similar amplitudes when $p = \mathcal{O}(\varepsilon \log(1/\varepsilon))$ (see equation (68)). Numerical simulations presented in Section 4 confirmed that breathing-kinks propagate as travelling waves for long periods of time with speed just below unity, and elementary analysis with wavenumbers p of the same order as the amplitude of the breather (ε) suggests that this should not fail before $t = \mathcal{O}(\varepsilon^{-2})$. The same timescale of validity is found, more rigorously, by Schneider & Wayne [25], and by Giannoulis & Mielke [13] for a related problem.

Combined breathing-kink modes have been observed in numerical simulations before, for instance, by Huang *et al.* [16], Wang [30], Gaididei *et al.* [11] and Bickham *et al.* [3]. However, a systematic theory giving their size, shape and speed has, until now, been lacking. We mention the work of Flytzanis *et al.* [10], who also find approximations to travelling breathers in this system, and the shape of breathing-kinks. We believe the treatment given here is simpler than that given by Flytzanis *et al.* [10] since we analyse the ϕ-equation (4) rather than the q-equation (2). Additionally, their solution ansatz assumes the existence of both an oscillatory and a slowly varying components with similar amplitudes. Explicitly, the ansatz of Flytzanis *et al.* [10] postulates the existence of both kink and breather components ($q_n \sim \varepsilon F_{10} + \varepsilon \mathrm{e}^{\mathrm{i}\omega t + \mathrm{i}pn} F_{11} + \mathcal{O}(\varepsilon^2) + \text{c.c.}$), implicitly assuming that their amplitudes have the same order of magnitude. Our approach also makes no assumption about the existence of moving breathing-kinks; we use a solution ansatz (11) which has only an oscillatory component, with the form $\phi \sim \varepsilon \mathrm{e}^{\mathrm{i}\omega t + \mathrm{i}pn} F + \mathcal{O}(\varepsilon^2) + \text{c.c.}$. The existence of a slowly varying component (which has the form of a kink) then arises naturally from our analysis. Furthermore, the amplitude of this resultant mode is determined as part of the problem and, whilst its amplitude *may* be comparable to that of the breather, in general, the amplitude takes values from $\mathcal{O}(1)$ to exponentially small in ε.

In closing, we discuss several advantages of the semi-discrete multiple-scale method of Remoissenet [20] over other early analytic methods. We believe the method of multiple scales in the semi-discrete limit to be a more rigorous, logical and systematic way of constructing approximate solutions than, for instance, the rotating-wave approximation (RWA) used widely in early analytic works (see Takeno *et al.* [28], or Bickham *et al.* [3]). Whilst the RWA yields similar results, it is an *ad hoc* method which typically only determines the leading-order approximation, and the accuracy of approximations made in the procedure are left unquantified. Problems with the RWA were originally highlighted by Hori & Takeno [15, 27] who noted that following the ansatz $u_n(t) = \phi_n(t) \cos(kn - \omega t)$ approximations such as $\phi_{n+1}^2 + \phi_{n-1}^2 + \phi_{n+1}\phi_{n-1} \approx 3\phi_n^2$, and $(\phi_{n+1} + \phi_{n-1})\phi_n \approx 2\phi_n^2$ whose accuracy is undetermined, are required.

In contrast, the method of asymptotic expansions retains information on the size of error terms and, by using an expansion, these error terms are corrected for in the calculation of terms of higher-order. A sequence of equations is solved to find a sequence of higher-order approximations. The validity of this method has recently been established rigorously by Giannoulis & Mielke [12, 13] for a related problem which includes an additional on-site potential, and by Schneider & Wayne [25]. It has also been applied successfully to higher-dimensional lattices, see, for example, Butt & Wattis [4, 5].

Acknowledgements

IAB would like to acknowledge financial assistance from the UK Engineering and Physical Sciences Research Council.

References

[1] S Aubry, G Kopidakis, and V Kadelburg. Variational proof for hard discrete breathers in some classes of Hamiltonian dynamical systems. *Disc. Cont. Dyn. Sys. B*, **1**, 271–298, (2001).

[2] O Bang and M Peyrard. Higher order breathers solutions to a discrete nonlinear Klein-Gordon model. *Physica D*, **81**, 9–22, (1995).

[3] SR Bickham, SA Kiselev, and Sievers AJ. Stationary and moving intrinsic localized modes in one-dimensional monatomic lattices with cubic and quartic anharmonicity. *Phys. Rev. B*, **47**, 14206–14211, (1993).

[4] IA Butt and JAD Wattis. Discrete breathers in a two-dimensional Fermi-Pasta-Ulam lattice. *J. Phys. A: Math. Gen.*, **39**, 4955–4984, (2006).

[5] IA Butt and JAD Wattis. Discrete breathers in a two-dimensional hexagonal Fermi-Pasta-Ulam lattice. *J. Phys. A: Math. Theor.*, **40**, 1239–1264, (2007).

[6] M Collins. A quasicontinuum approximation for solitons in an atomic chain. *Chem. Phys. Lett.*, **77**, 342–347, (1981).

[7] M Collins and S Rice. Some properties of large amplitude motion in an anharmonic chain with nearest neighbor interactions. *J. Chem. Phys.*, **67**, 2607–2622, (1982).

[8] E Fermi, J Pasta, and S Ulam. Studies of nonlinear problems. Los Alamos Scientific Report, (1940), originally unpublished. Later published in Lectures in Applied Mathematics, **15**, 143–156, (1974).

[9] S Flach. Existence of localized excitations in nonlinear Hamiltonian lattices. *Phys. Rev. E*, **51**, 1503–1507, (1995).

[10] N Flytzanis, S Pnevmatikos, and M Remoissenet. Kink, breather and asymmetric envelope or dark solitons in nonlinear chains I: monatomic chain. *J. Phys. C: Sol. St. Phys.*, **18**, 4603–4629, (1985).

[11] Y Gaididei, R Huß, and FG Mertens. Envelope solitary waves on two-dimensional lattices with in-plane displacements. *Euro. Phys. Journ. B*, **6**, 257–271, (1998).

[12] J Giannoulis and A Mielke. The nonlinear Schrödinger equation as a macroscopic limit for an oscillator chain with cubic nonlinearities. *Nonlinearity*, **17**, 551–565, (2004).

[13] J Giannoulis and A Mielke. Dispersive evolution of pulses in oscillator chains with general interaction potentials. *Disc. Cont. Dyn. Sys. B*, **6**, 493–523, (2006).

[14] IS Gradshteyn and IM Ryzhik. *Table of Integrals, Series and Products, sixth edition*. Academic Press, London, (2000).

[15] K Hori and S Takeno. Moving self-localized modes for the displacement field in a one-dimensional lattice system with quartic anharmonicity. *J. Phys. Soc. Japan*, **61**, 2186–2189, (1992).

[16] G Huang, Z Shi, and Z Xu. Asymmetric intrinsic localized modes in a homogeneous lattice with cubic and quartic anharmonicity. *Phys. Rev. B*, **47**, 14561, (1993).

[17] G James. Existence of breathers on FPU lattices. *C. R. Acad. Sci. Paris*, **332**, 581–586, (2001).

[18] RS MacKay and S Aubry. Proof of existence of breathers for time-reversible or Hamiltonian networks of weakly coupled oscillators. *Nonlinearity*, **7**, 1623–1643, (1984).

[19] M Remoissenet. Low-amplitude breather and envelope solitons in quasi-one-dimensional physical models. *Phys. Rev. B*, **33**, 2386–2392, (1985).

[20] M Remoissenet. *Waves Called Solitons. Concepts and Experiments, third edition*. Springer-Verlag, Berlin, (1999).

[21] P Rosenau. Dynamics of nonlinear mass-spring chains near the continuum limit. *Phys. Lett. A*, **118**, 222–227, (1986).

[22] P Rosenau. Dynamics of dense lattices. *Phys. Rev. B*, **36**, 5868–5876, (1987).

[23] B Sánchez-Rey, G James, J Cuevas, and JFR Archilla. Bright and dark breathers in Fermi-Pasta-Ulam lattices. *Phys. Rev. B*, **70**, 014301, (2004).

[24] KW Sandusky, JB Page, and KE Schmidt. Stability and motion of intrinsic localized modes in nonlinear periodic lattices. *Phys. Rev. B*, **46**, 6161–6168, (1992).

[25] G Schneider and CE Wayne. Counter-propagating waves on fluid surfaces and the continuum limit of the Fermi-Pasta-Ulam model, pp390–404 of B Fiedler, K Gröger, J Sprekels (eds) International Conference on Differential Equations, World Scientific, River Edge, NJ, (2000).

[26] AC Scott. *Nonlinear Science, second edition*. Oxford University Press, Oxford, (1999).

[27] S Takeno and K Hori. A propagating self-localized mode in a one-dimensional lattice with quartic anharmonicity. *J. Phys. Soc. Japan*, **59**, 3037–3040, (1990).

[28] S Takeno, K Kisoda, and AJ Sievers. Intrinsic localized vibrational modes

in anharmonic crystals. *Prog. Theor. Phys. Suppl.*, **94**, 242–269, (1988).
[29] M Toda. *Theory of Nonlinear Lattices*. Springer, Berlin, (1978).
[30] S Wang. Influence of cubic anharmonicity on high frequency modes. *Phys. Lett. A*, **200**, 103–108, (1995).
[31] JAD Wattis. Approximations to solitary waves on lattices. II. quasi-continuum methods for fast and slow waves. *J. Phys. A: Math. Gen.*, **26**, 1193–1209, (1993).
[32] JAD Wattis. Variational approximations to breathers in the discrete sine-Gordon equation II: moving breathers and Peierls-Nabarro energies. *Nonlinearity*, **9**, 1583–1598, (1996).
[33] JAD Wattis. Stationary breather modes of generalized nonlinear Klein-Gordon lattices. *J. Phys. A: Math. Gen.*, **31**, 3301–3323, (1998).